OPEN ACCESS Freely available online

PLOS ONE

Three-Dimensional Flow of an Oldroyd-B Nanofluid towards Stretching Surface with Heat Generation/ Absorption

Waqar Azeem Khan*, Masood Khan, Rabia Malik

Department of Mathematics, Quaid-i-Azam University, Islamabad, Pakistan

Abstract

This article addresses the steady three-dimensional flow of an Oldroyd-B nanofluid over a bidirectional stretching surface with heat generation/absorption effects. Suitable similarity transformations are employed to reduce the governing partial differential equations into coupled nonlinear ordinary differential equations. These nonlinear ordinary differential equations are then solved analytically by using the homotpy analysis method (HAM). Graphically results are presented and discussed for various parameters, namely, Deborah numbers β_1 and β_2, heat generation/absorption parameter λ, Prandtl parameter Pr, Brownian motion parametersN_b, thermophoresis parameter N_t and Lewis number Le. We have seen that the increasing values of the Brownian motion parameter N_t and thermophoresis parameter N_t leads to an increase in the temperature field and thermal boundary layer thickness while the opposite behavior is observed for concentration field and concentration boundary layer thickness. To see the validity of the present work, the numerical results are compared with the analytical solutions obtained by Homotopy analysis method and noted an excellent agreement for the limiting cases.

Citation: Azeem Khan W, Khan M, Malik R (2014) Three-Dimensional Flow of an Oldroyd-B Nanofluid towards Stretching Surface with Heat Generation/ Absorption. PLoS ONE 9(8): e105107. doi:10.1371/journal.pone.0105107

Editor: Mark G. Kuzyk, Washington State University, United States of America

Received March 3, 2014; **Accepted** July 20, 2014; **Published** August 29, 2014

Funding: This work has the financial support of the Higher Education Commission (HEC) of Pakistan. The funders had no role in study design, data collection and analysis, decision to publish, or preparation of the manuscript.

Competing Interests: The authors have declared that no competing interests exist.

* Email: Waqar_qau85@yahoo.com

Introduction

During the past few years, study of the boundary layer flow of nanofluids over a linear stretching surface has become more and more attractive because of its numerous applications in industrial manufacturing. With regard to the sundry application of nanofluids, the researchers have been given considerable attention to improve heat transfer using nanofluids. Regular fluids, such as ethylene, water, glycol mixture and some types of oil have low heat transfer rates. Therefore it is necessary to improve some physical properties such as thermal conductivity and heat transfer rate of conventional fluids by the utilization of nanoparticles in base fluid. The term nanofluid was first time introduced by Choi [1]. In another paper, Choi et al. [2] observed that thermal conductivity of pure fluid can be increased by a factor of 2 with an addition of one percent by volume fraction of the nanoparticle.

Sakiadis [3] was the first who investigated the boundary layer flow on a continuous stretching surface. In his paper, he provided numerical solutions of the boundary layer flow over a continuous stretching surface. Later on Crane [4] analyzed the exact solution of boundary layer flow of Newtonian fluid due to stretching of an elastic sheet moving linearly in its own plane. Wang [5] investigated the free convection on a vertical stretching surface. Heat transfer analysis over an exponentially stretching continuous surface was analyzed by Elbashbeshy [6]. Rana and Kango [7] discussed the effect of rotation on thermal instability of compressible Walters' (model) elastico-viscous fluid in porous medium. Heat transfer over a stretching surface with variable heat flux in micropolar fluids was presented by Ishak et al. [8]. Chamkha and Aly [9] examined MHD free convective boundary layer flow of a nanofluid along a permeable isothermal vertical plate in the presence of heat source or sink. Thermosolutal convection in Walters' (Model B') elastico-viscous rotating fluid permeated with suspended particles and variable gravity field in porous medium in hydromagnetics was investigated by Rana [10]. Matin et al. [11] presented the MHD mixed convective flow of a nanofluid over a stretching sheet. Chand and and Rana [12] examined the oscillating convection of nanofluid in porous medium. Aziz and Khan [13] studied natural convective flow of a nanofluid over a convectively heated vertical plate. Kuznetsov and Nield [14] analyzed the natural convective flow of a nanofluid past a vertical plate. Khan and Pop [15,16] investigated the laminar flow of nanofluids past a stretching sheet. Hamad et al. [17] formulated the problem of free convective flow of nanofluid past a semi-infinite vertical plate with influence of magnetic field. Hady et al. [18] investigated the effects of thermal radiation on the viscous flow of a nanofluid and heat transfer over a non-linear sheet. Makinde and Aziz [19] performed the numerical study of boundary layer over a linear stretching sheet. Cheng [20] analyzed the behavior of boundary layer flow over a horizontal cylinder of elliptic cross section in a porous. Narayana and Sibanda [21] elaborated the effects of laminar flow of a nanofluid over an unsteady stretching sheet. Kameswaran et al. [22] investigated flow due to a stretching or shrinking sheet with viscous dissipation and chemical reaction effects. The effects of an unsteady boundary-layer flow and heat transfer of a nanofluid over a

porous stretching/shrinking sheet have been investigated by Bachok et al. [23]. Hamad and Ferdows [24] presented the similarity solutions for viscous flow and heat transfer of a nanofluid over a non-linear stretching sheet. The studies on heat generation/absorption effects for boundary layer flow of nanofluids are very limited. Recently, Alsaedi et al. [25] investigated the effects of heat generation/absorption on stagnation point flow of nanofluid over a surface with convective boundary conditions. Thermal instability of Rivlin-Ericksen Elastico-Viscous nanofluid saturated by a porous medium were presented by Chand and Rana [26]. On the onset of thermal convection in rotating nanofluid layer saturating a Darcy-Brinkman porous medium were studied by Chand and Rana [27]. Nandy and Mahapatra [28] examined the effects of slip and heat generation/absorption on MHD stagnation point flow of nanofluid past a stretching/shrinking surface with convective boundary conditions. On the onset of thermosolutal instability in a layer of an Elastico-Viscous nanofluid in porous medium was investigated by Rana et al. [29].

However, to the best of author's knowledge, no attempts have thus far been communicated with regards to free convective boundary layer flow of three-dimensional Oldroyd-B nanofluid over a stretching surface. The aim of the present article is to study the free convective boundary-layer flow of three-dimensional Oldroyd-B nanofluid fluid flow over a stretching sheet. The Oldroyd-B fluid model was employed to describe rheological behavior of viscoelastic nanofluid. The Oldroyd-B fluid model is important because of its applications in the production of plastic sheet and extrusion of polymers through through a slit die in polymer industry. The considered stretched flow problem involves problem involves the significant heat transfer between the sheet and the surrounding fluid. The extrudate in this mechanism starts to solidify as soon as it exits from the die and then sheet is collected by a wind-up roll upon solidification. Physical properties of the cooling medium, e.g., its thermal conductivity has pivotal role in such process. The success of whole operation closely depends upon the viscoelastic character of fluid above the sheet. By applying boundary layer approximations a system of nonlinear partial differential equations is obtained. Then, invoking suitable similarity transformations, we reduced the system into nonlinear ordinary differential equations. This system of coupled nonlinear ordinary differential equations is then solved analytically by using the homotpoy analysis method (HAM). The variations of different flow controlling parameters on the velocity, temperature and concentration profiles are addressed.

Mathematical Formulation

Consider a steady three-dimensional (x, y, z) free convective boundary layer flow of an incompressible Oldroyd-B nanofluid over a stretching sheet kept at a constant temperature T_w and concentration C_w. The ambient temperature and concentration far away from the sheet are taken as T_∞ and C_∞, respectively. The flow is due to a bidirectional stretched surface at $z=0$. The governing equations for the steady three-dimensional flow of an Oldroyd-B nanofluid, approximated by boundary-layer theory, are [30]

$$\frac{\partial u}{\partial x}+\frac{\partial v}{\partial y}+\frac{\partial w}{\partial z}=0, \tag{1}$$

$$\begin{aligned}&u\frac{\partial u}{\partial x}+v\frac{\partial u}{\partial y}+w\frac{\partial u}{\partial z}+\\&\lambda_1\left(u^2\frac{\partial^2 u}{\partial x^2}+v^2\frac{\partial^2 u}{\partial y^2}+w^2\frac{\partial^2 u}{\partial z^2}+2uv\frac{\partial^2 u}{\partial x\partial y}\right)+\\&2vw\frac{\partial^2 u}{\partial y\partial z}+2uw\frac{\partial^2 u}{\partial x\partial z}\\&=\nu\left[\frac{\partial^2 u}{\partial z^2}+\lambda_2\left(u\frac{\partial^3 u}{\partial x\partial z^2}+v\frac{\partial^3 u}{\partial y\partial z^2}+w\frac{\partial^3 u}{\partial z^3}-\frac{\partial u\partial^2 u}{\partial x\partial z^2}\right)\right]-\\&\frac{\partial u\partial^2 v}{\partial y\partial z^2}-\frac{\partial u\partial^2 w}{\partial z\partial z^2},\end{aligned} \tag{2}$$

$$\begin{aligned}&u\frac{\partial v}{\partial x}+v\frac{\partial v}{\partial y}+w\frac{\partial v}{\partial z}+\\&\lambda_1\left(u^2\frac{\partial^2 v}{\partial x^2}+v^2\frac{\partial^2 v}{\partial y^2}+w^2\frac{\partial^2 v}{\partial z^2}+2uv\frac{\partial^2 v}{\partial x\partial y}\right)+\\&2vw\frac{\partial^2 v}{\partial y\partial z}+2uw\frac{\partial^2 v}{\partial x\partial z}\\&=\nu\left[\frac{\partial^2 v}{\partial z^2}+\lambda_2\left(u\frac{\partial^3 v}{\partial x\partial z^2}+v\frac{\partial^3 v}{\partial y\partial z^2}+w\frac{\partial^3 v}{\partial z^3}-\frac{\partial v\partial^2 v}{\partial x\partial z^2}\right)\right]\\&-\frac{\partial v\partial^2 v}{\partial y\partial z^2}-\frac{\partial v\partial^2 w}{\partial z\partial z^2},\end{aligned} \tag{3}$$

$$\begin{aligned}&u\frac{\partial T}{\partial x}+v\frac{\partial T}{\partial y}+w\frac{\partial T}{\partial z}=\\&\alpha\frac{\partial^2 T}{\partial z^2}+\frac{Q_0}{\rho C_p}(T-T_\infty)+\tau\left[D_B\frac{\partial C}{\partial z}\frac{\partial T}{\partial z}+\frac{D_T}{T_\infty}\left(\frac{\partial T}{\partial z}\right)^2\right],\end{aligned} \tag{4}$$

$$u\frac{\partial C}{\partial x}+v\frac{\partial C}{\partial y}+w\frac{\partial C}{\partial z}=D_B\frac{\partial^2 C}{\partial z^2}+\frac{D_T}{T_\infty}\frac{\partial^2 T}{\partial z^2}. \tag{5}$$

Here (u, v, w) are velocity components, T the temperature, C the concentration, λ_1 and λ_2 the relaxation and retardation times respectively, ρ the fluid density, α the thermal diffusivity, Q_0 the heat generation/absorption parameter, τ the ratio of effective heat capacity of the nanoparticle material to the heat capacity of the fluid, D_B the Brownian diffusion coefficient and D_T the thermophoresis diffusion coefficient.

Equations (1) to (5) are subjected to the following boundary conditions

$$u=ax, v=by, w=0, T=T_w, C=C_w \text{ at } z=0, \tag{6}$$

Table 1. Convergence of the homotopy solutions when $\beta_1=\beta_2=0.2, \beta=0.4$, $\Pr=1.2, N_b=N_t=0.1$ and $L_e=1$ are fixed.

Order of approximation	$-f''(0)$	$-g''(0)$	$-\theta'(0)$	$-\varphi'(0)$
1	1.00420	0.337840	0.622000	0.352000
5	1.02196	0.328912	0.549080	0.493576
10	1.02155	0.328848	0.549423	0.489147
15	1.02154	0.328870	0.549446	0.488882
20	1.02154	0.328869	0.549438	0.488934
26	1.02154	0.328869	0.549438	0.488939
30	1.02154	0.328869	0.549438	0.488939
35	1.02154	0.328869	0.549438	0.488939

doi:10.1371/journal.pone.0105107.t001

$$u\to 0, v\to 0, T\to T_\infty, C\to C_\infty \text{ as } z\to\infty. \tag{7}$$

The similarity variables are introduced as

$$u(x,y)=axf'(\eta), v(x,y)=ayg'(\eta), w=-\sqrt{av}[f(\eta)+g(\eta)]$$
$$\theta(\eta)=\frac{T-T_\infty}{T_w-T_\infty}, \phi(\eta)=\frac{C-C_\infty}{C_w-C_\infty}, \eta=z\sqrt{\frac{a}{v}}, \tag{8}$$

and Eqs.(1)–(7) can be cast as

$$f'''+(f+g)f''-f'^2+\beta_1\left[2(f+g)f'f''-(f+g)^2f'''\right]+\beta_2\left[2(f''+g'')f''-(f+g)f^{iv}\right]=0, \tag{9}$$

$$g'''+(f+g)g''-g'^2+\beta_1\left[2(f+g)g'g''-(f+g)^2g'''\right]+\beta_2\left[2(f''+g'')g''-(f+g)g^{iv}\right]=0, \tag{10}$$

$$\theta''+\Pr(f+g)\theta'+\Pr N_b\phi'\theta'+\Pr N_t\theta'^2+\Pr\lambda\theta=0, \tag{11}$$

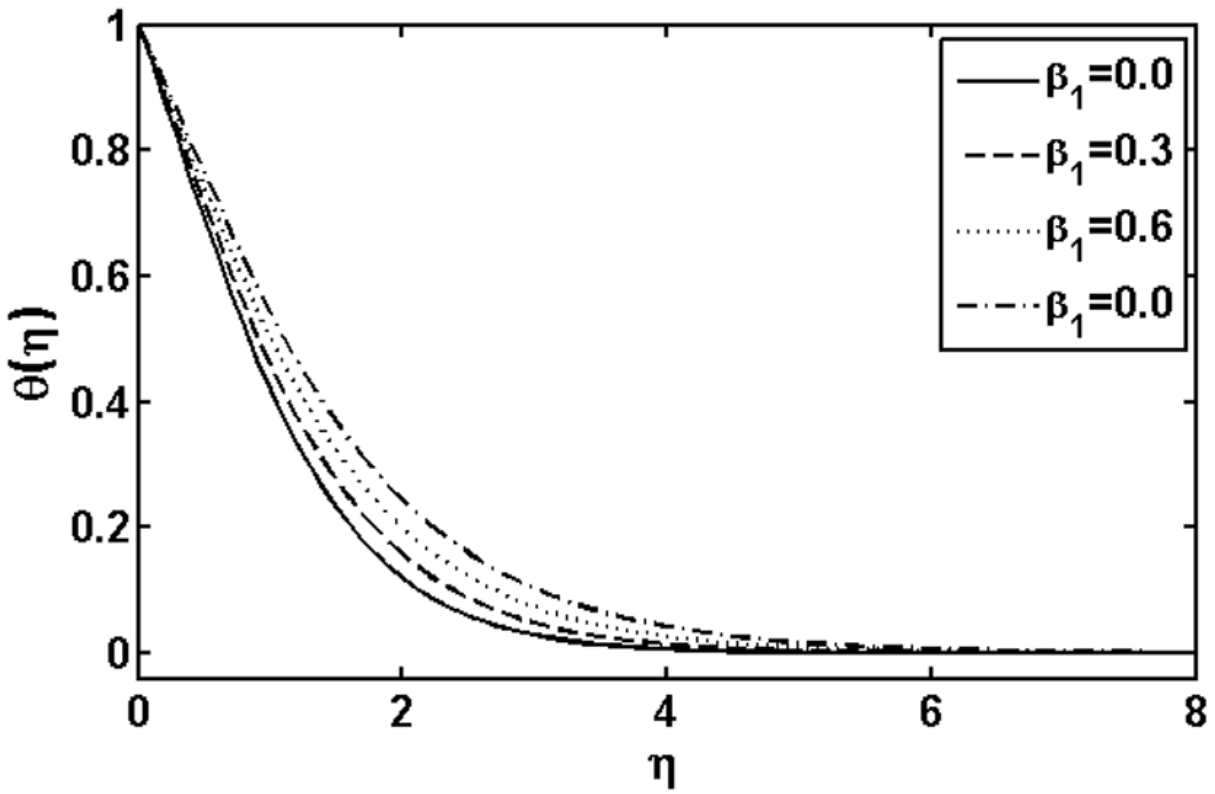

Figure 1. Variation of β_1 on $\theta(\eta)$ when $\beta_2=0.2, \beta=0.4$, $\Pr=0.4, \lambda=0.2, N_b=N_t=0.1$ and $Le=1.0$ are fixed.
doi:10.1371/journal.pone.0105107.g001

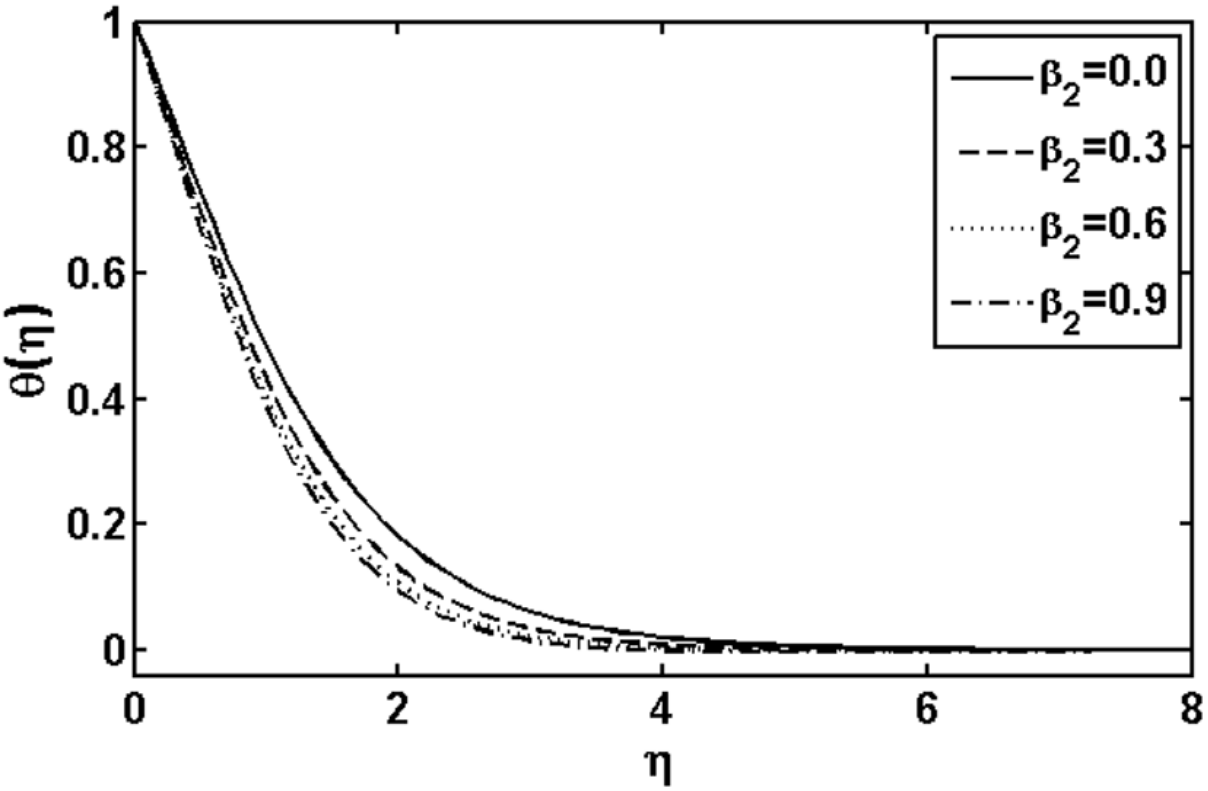

Figure 2. Variation of β_2 on $\theta(\eta)$ when $\beta_1 = 0.2, \beta = 0.4,\ \mathrm{Pr} = 0.4, \lambda = 0.2, N_b = N_t = 0.1$ and $Le = 1.0$ are fixed.
doi:10.1371/journal.pone.0105107.g002

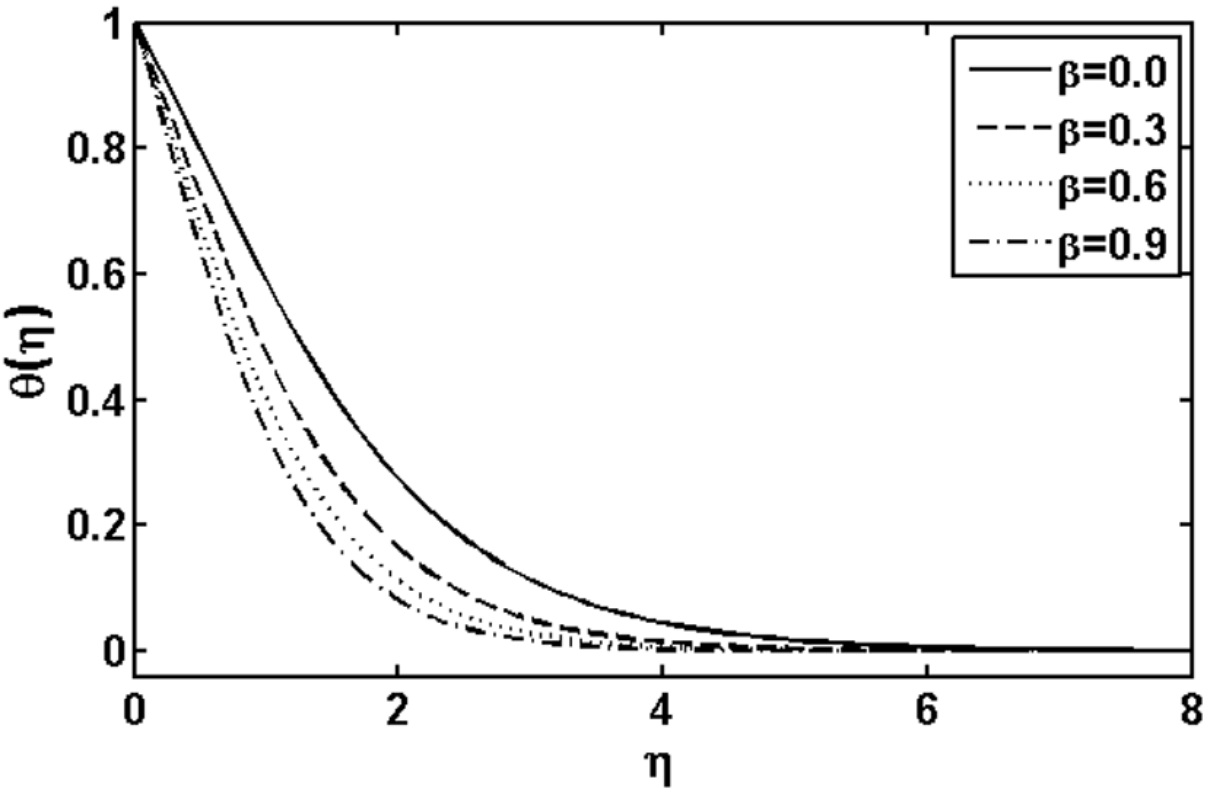

Figure 3. Variation of β on $\theta(\eta)$ when $\beta_1 = \beta_2 = 0.2, \beta = 0.4,\ \mathrm{Pr} = 1.2, \lambda = 0.2, N_b = N_t = 0.1$ and $Le = 1.0$ are fixed.
doi:10.1371/journal.pone.0105107.g003

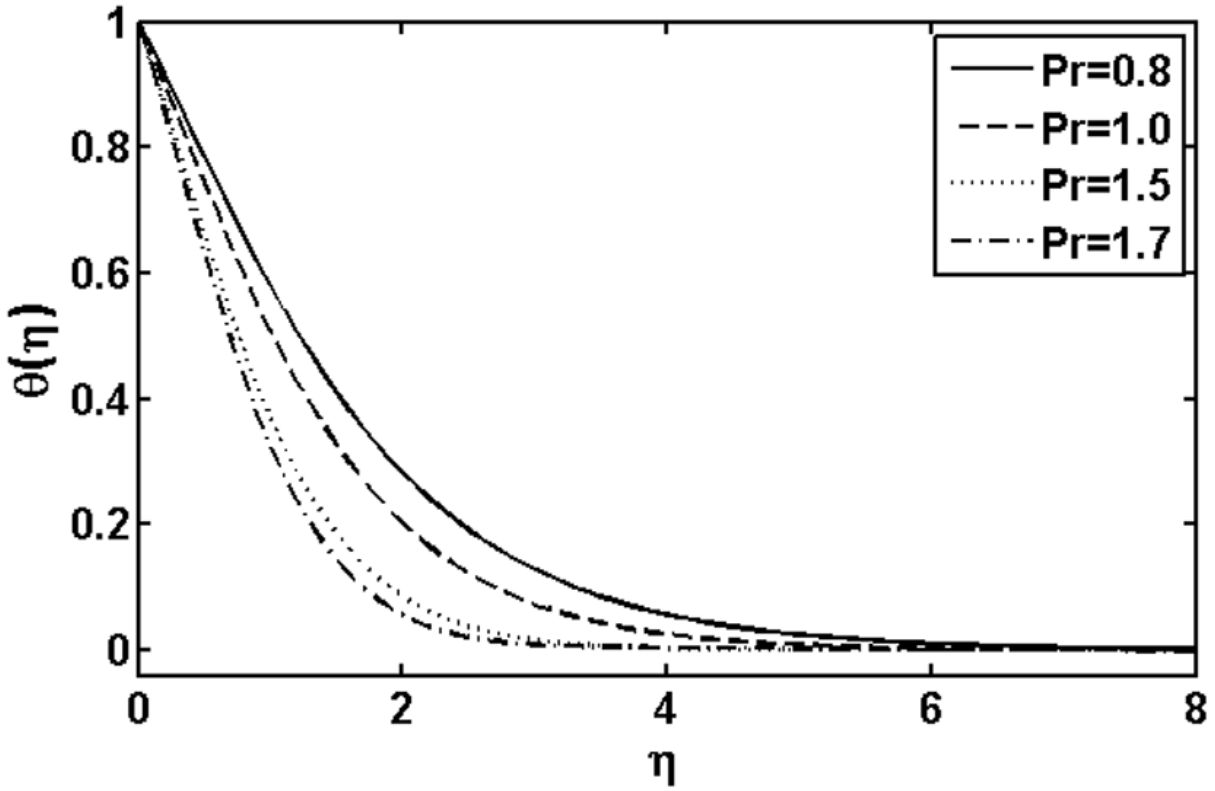

Figure 4. Variation of $\Pr$ **on** $\theta(\eta)$ **when** $\beta_1=\beta_2=0.2, \beta=0.2, \lambda=0.2, N_b=N_t=0.1$ **and** $Le=1.0$ **are fixed.**
doi:10.1371/journal.pone.0105107.g004

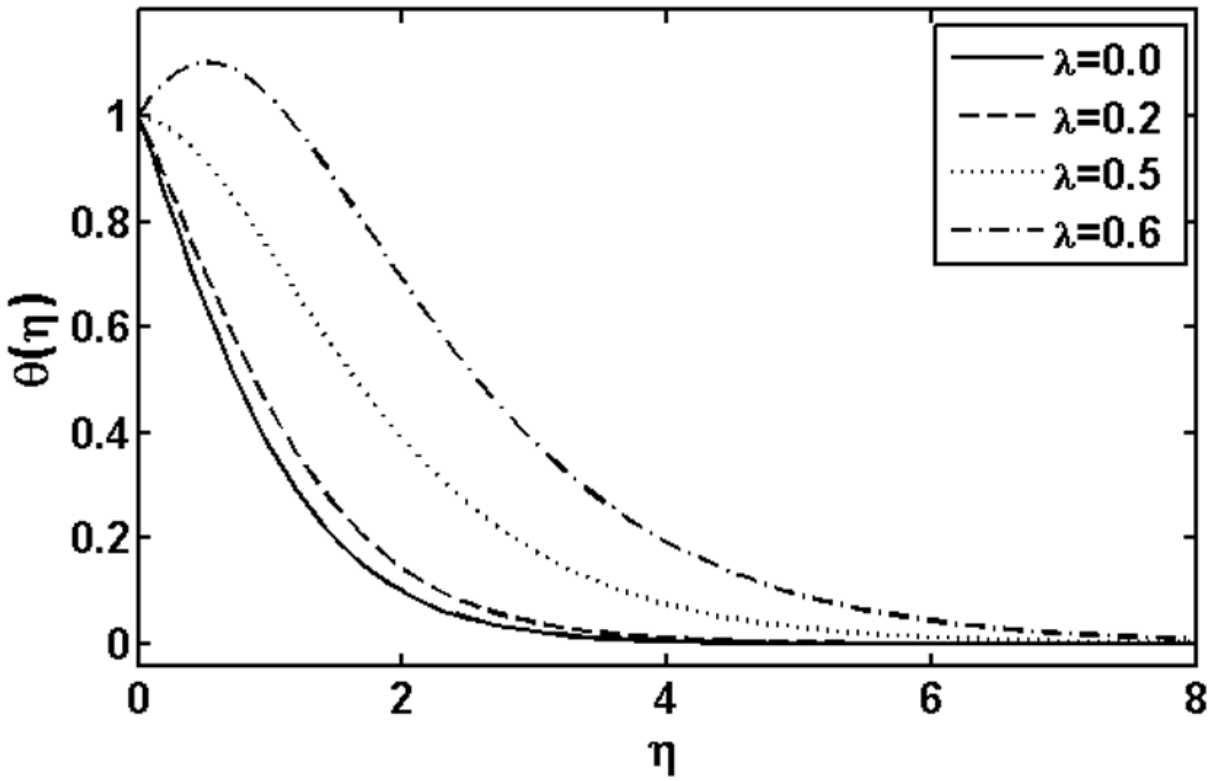

Figure 5. Variation of λ **on** $\theta(\eta)$ **when** $\beta_1=\beta_2=0.2, \beta=0.4, \Pr=1.2, N_b=N_t=0.1$ **and** $Le=1.0$ **are fixed.**
doi:10.1371/journal.pone.0105107.g005

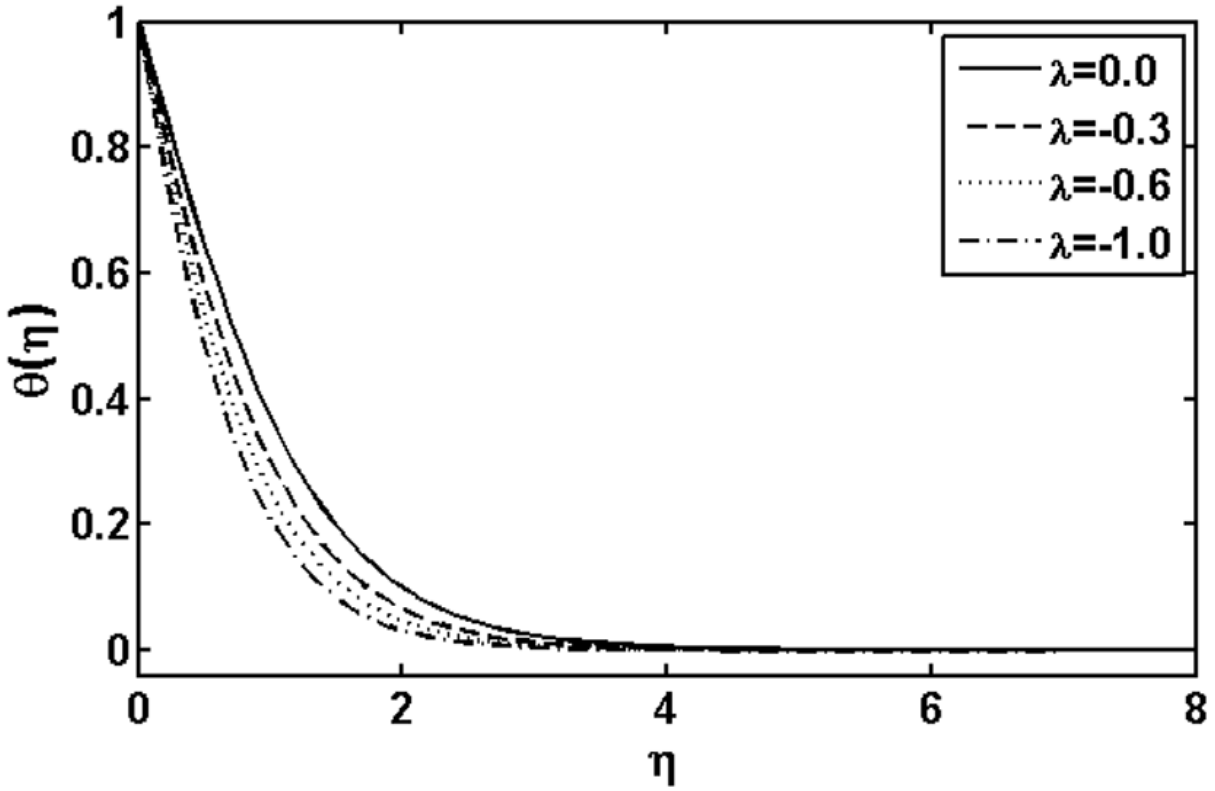

Figure 6. Variation of λ on $\theta(\eta)$ when $\beta_1 = \beta_2 = 0.2, \beta = 0.4,\ \mathrm{Pr} = 1.2, N_b = N_t = 0.1$ and $Le = 1.0$ are fixed.
doi:10.1371/journal.pone.0105107.g006

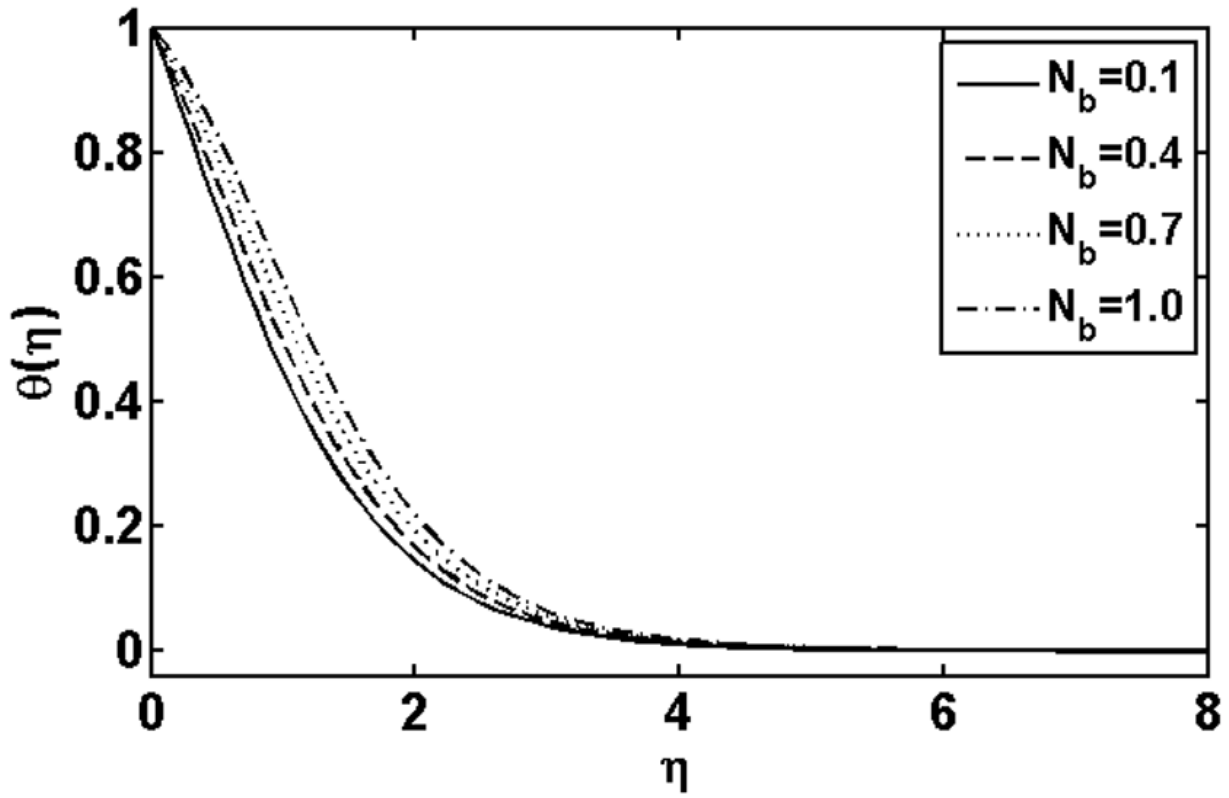

Figure 7. Variation of N_b on $\theta(\eta)$ when $\beta_1 = \beta_2 = 0.2, \beta = 0.4,\ \mathrm{Pr} = 1.2, \lambda = 0.2, N_t = 0.1$ and $Le = 1.0$ are fixed.
doi:10.1371/journal.pone.0105107.g007

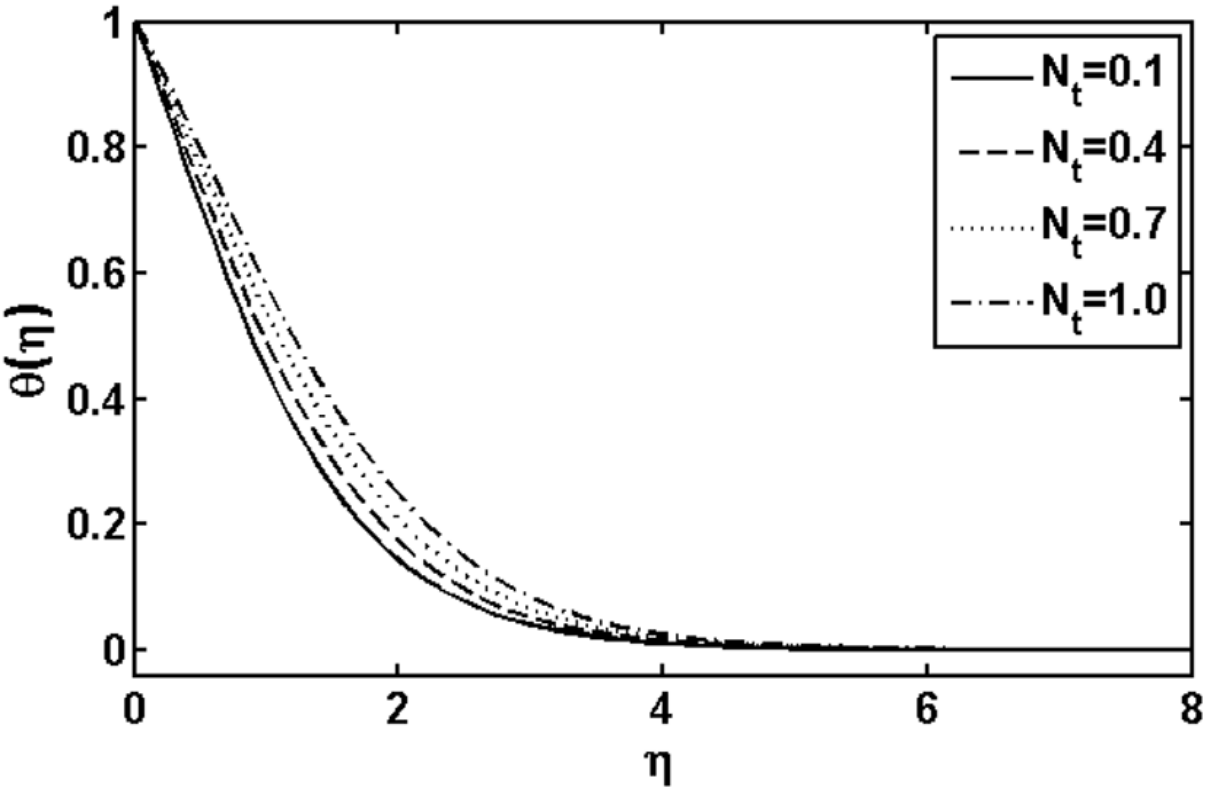

Figure 8. Variation of N_t on $\theta(\eta)$ when $\beta_1=\beta_2=0.2, \beta=0.4,\ \mathrm{Pr}=1.2, \lambda=0.2, N_b=0.1$ and $Le=1.0$ are fixed.
doi:10.1371/journal.pone.0105107.g008

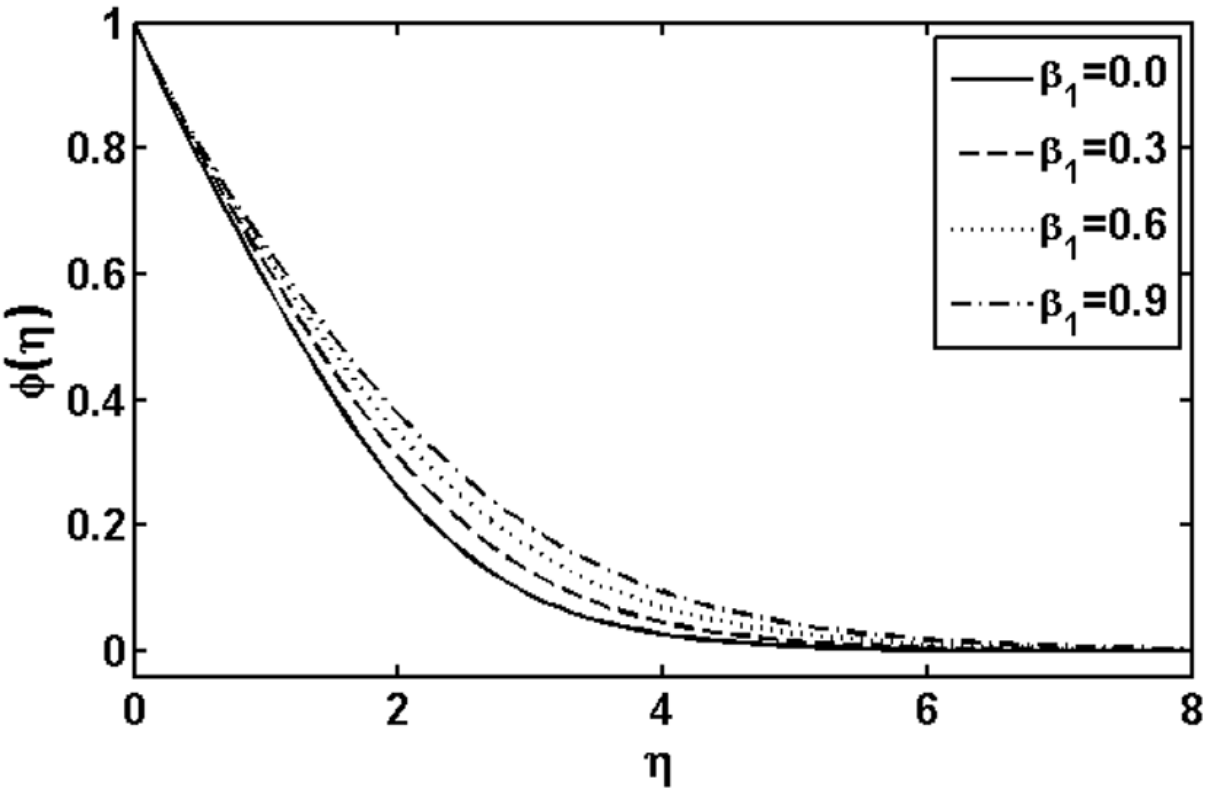

Figure 9. Variation of β_1 on $\vartheta(\eta)$ when $\beta_2=0.2, \beta=0.4,\ \mathrm{Pr}=1.2, \lambda=0.2, N_b=N_t=0.1$ and $Le=1.0$ are fixed.
doi:10.1371/journal.pone.0105107.g009

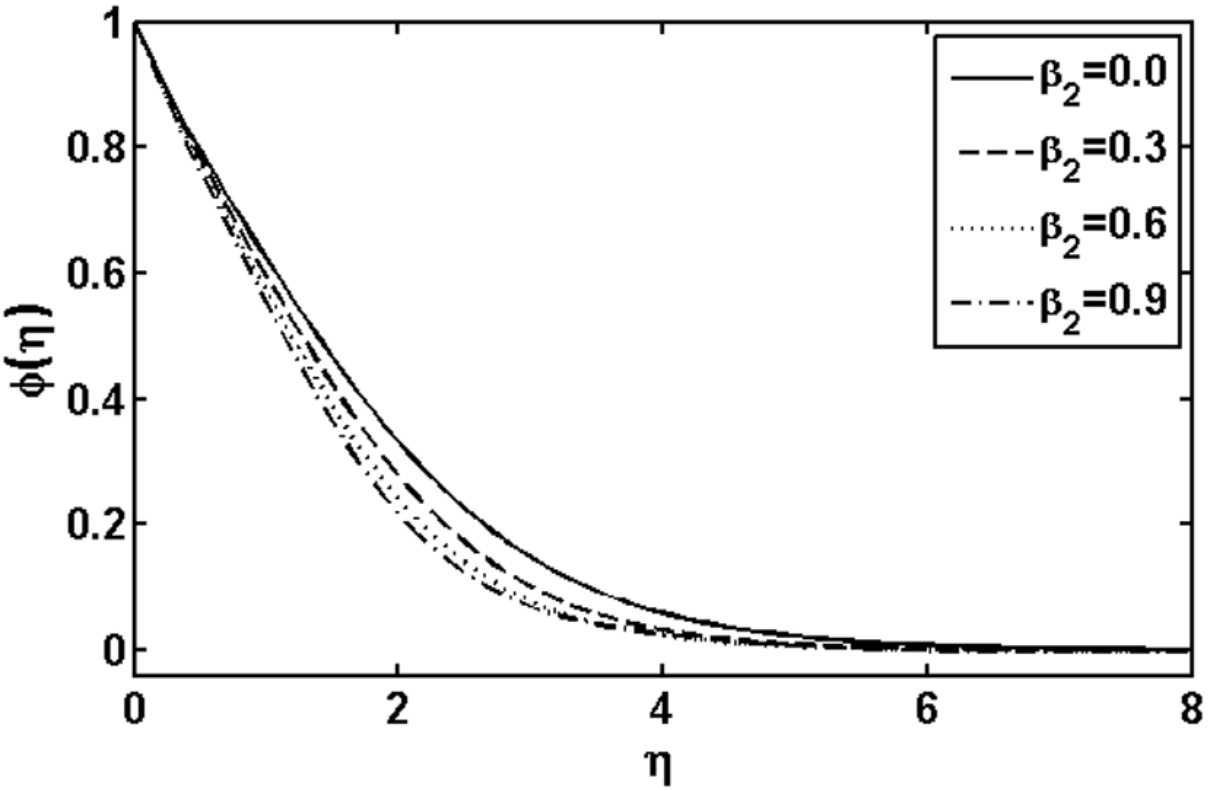

Figure 10. Variation of β_2 on $\vartheta(\eta)$ when $\beta_1 = 0.2, \beta = 0.4,\ \mathrm{Pr} = 1.2, \lambda = 0.2, N_b = N_t = 0.1$ and $Le = 1.0$ are fixed.
doi:10.1371/journal.pone.0105107.g010

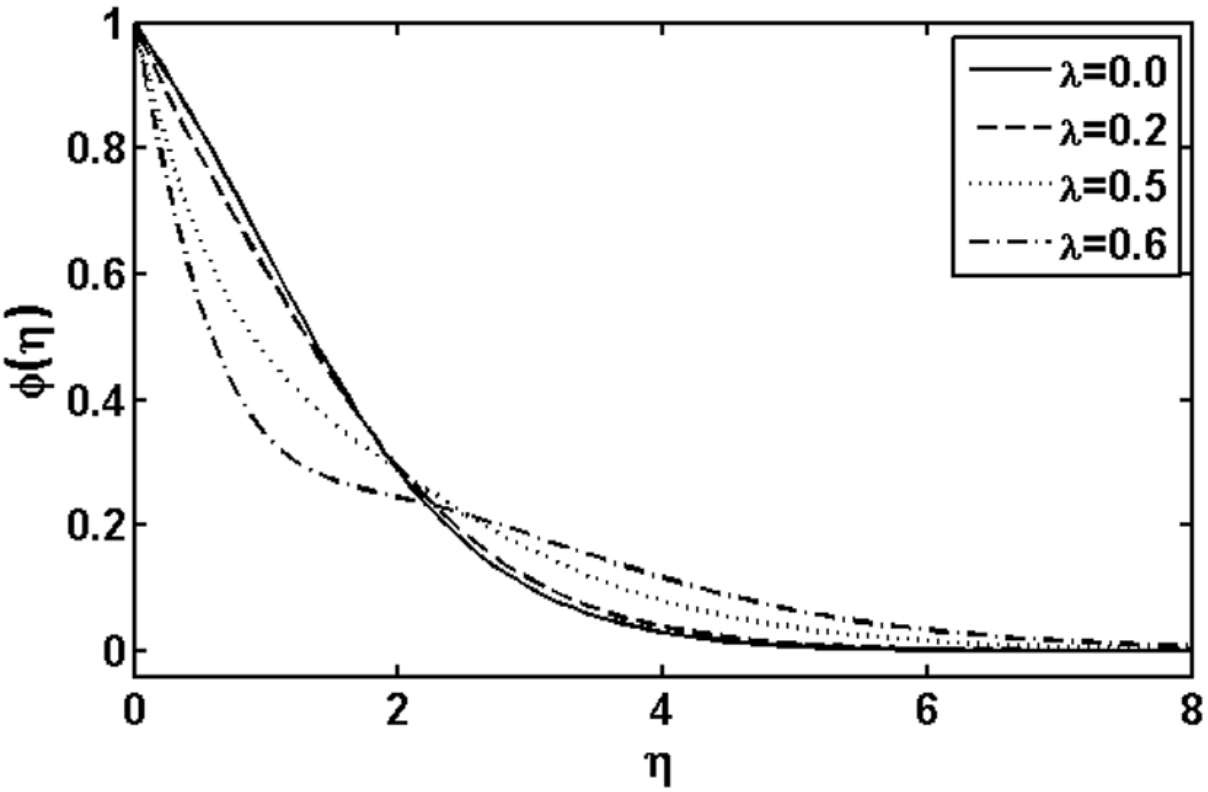

Figure 11. Variation of λ on $\vartheta(\eta)$ when $\beta_1 = \beta_2 = 0.2, \beta = 0.4,\ \mathrm{Pr} = 1.2, N_b = N_t = 0.1$ and $Le = 1.0$ are fixed.
doi:10.1371/journal.pone.0105107.g011

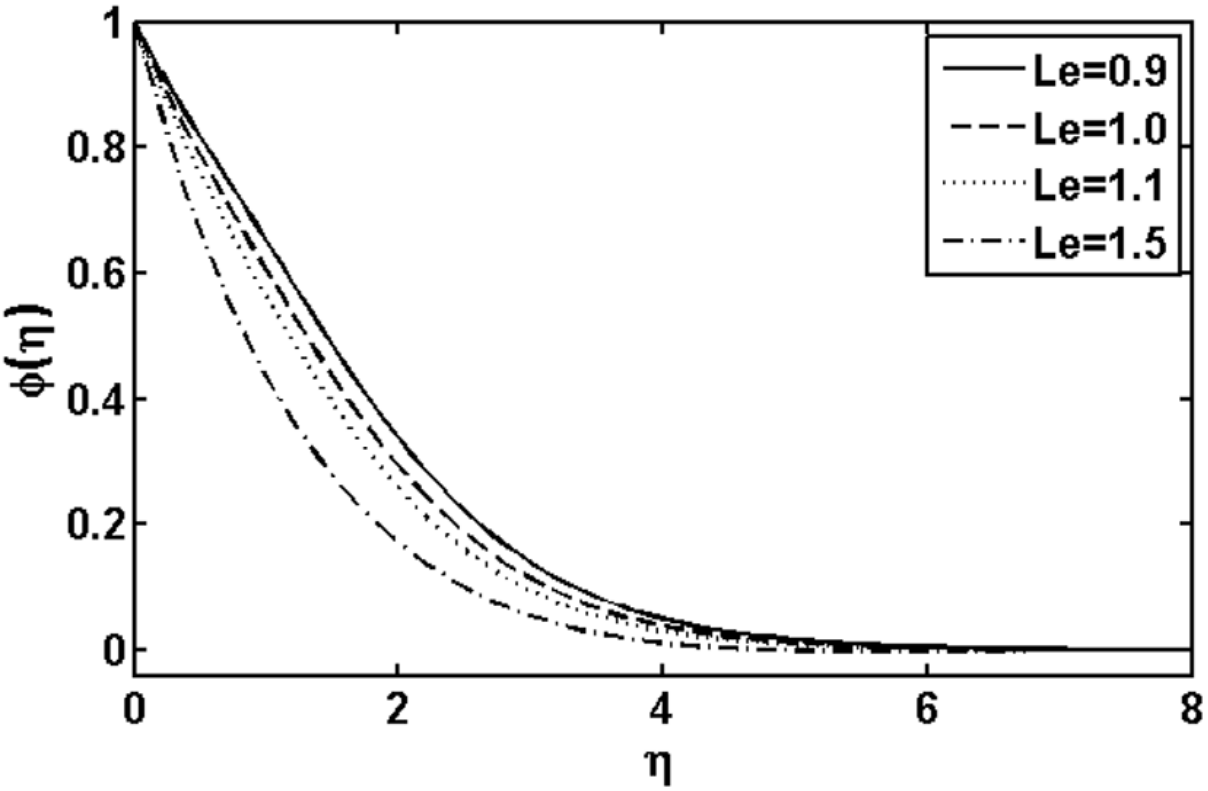

Figure 12. Variation of Le on $\vartheta(\eta)$ when $\beta_1=\beta_2=0.2, \beta=0.4,\ \mathrm{Pr}=1.2, \lambda=0.2, N_b=0.1,$ and $N_t=0.1$ are fixed.
doi:10.1371/journal.pone.0105107.g012

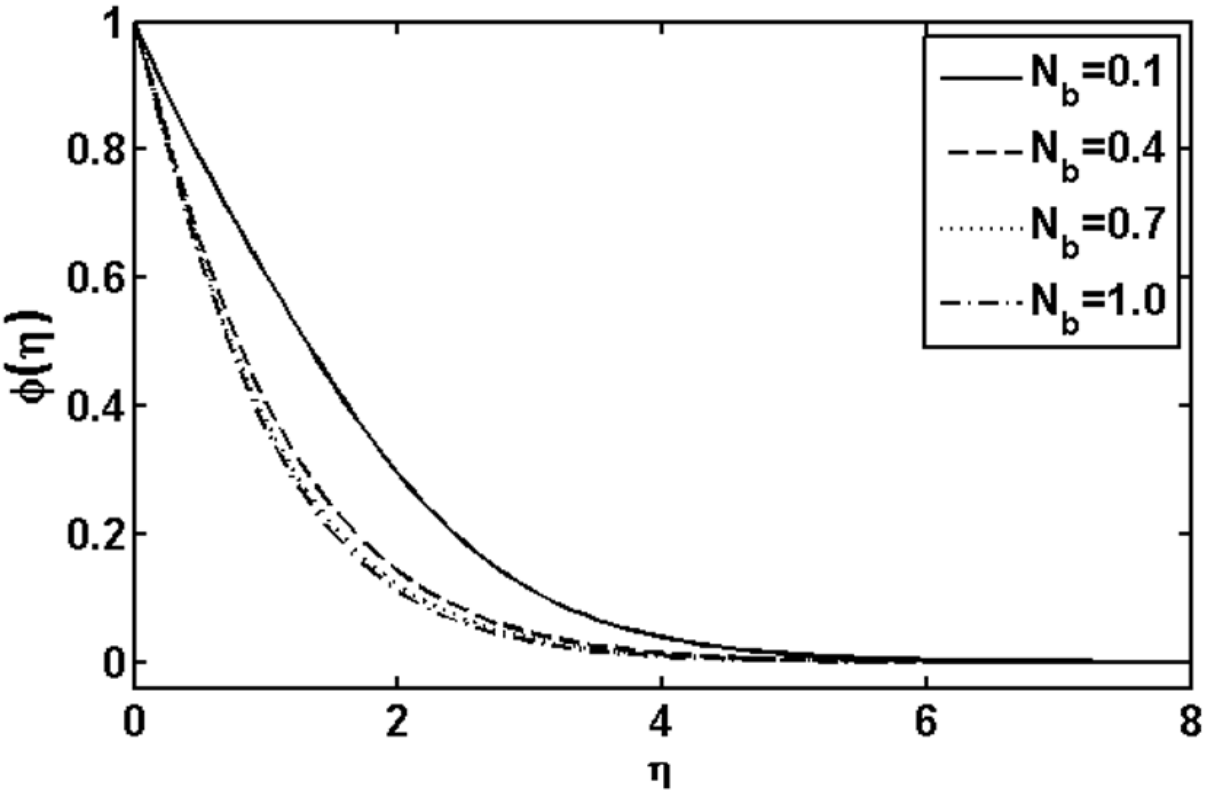

Figure 13. Variation of N_b on $\vartheta(\eta)$ when $\beta_1=\beta_2=0.2, \beta=0.4,\ \mathrm{Pr}=1.2, \lambda=0.2, N_t=0.1$ and $Le=1.0$ are fixed.
doi:10.1371/journal.pone.0105107.g013

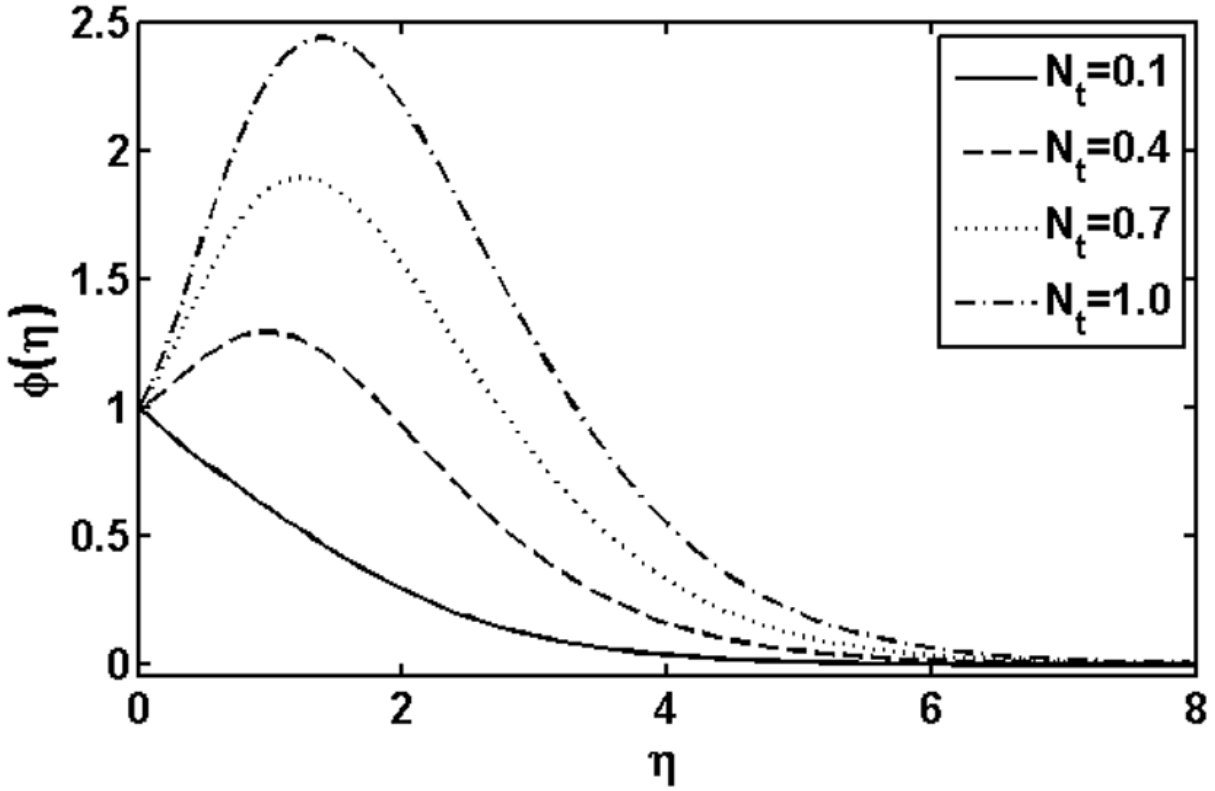

Figure 14. Variation of N_t on $\vartheta(\eta)$ when $\beta_1=\beta_2=0.2, \beta=0.4$, Pr $=1.2, \lambda=0.2, N_b=0.1$ and $Le=1.0$ are fixed.
doi:10.1371/journal.pone.0105107.g014

$$\phi''+\underset{L}{\Pr} e(f+g)\phi'+\frac{N_t}{N_b}\theta''=0, \tag{12}$$

$$f=0, g=0, f'=1, g'=\beta, \theta=1, \vartheta=1 \text{ at } \eta=0, \tag{13}$$

$$f'\to 0, g'\to 0, \theta\to 0, \phi\to 0 \text{ as } \eta\to\infty, \tag{14}$$

where prime denotes differentiation with respect to η. Moreover, β_1 and β_2 are the Deborah numbers, β the ratio of stretching rates parameter, Pr the generalized Prandtl number, λ the heat source ($\lambda>0$) and the heat sink ($\lambda<0$) parameter, N_b the local Brownian motion parameter, N_t the local thermophoresis parameter and Le the Lewis number which are defined as

Table 2. A comparison for the velocity gradients for different values of β when $\beta_1=\beta_2=0$ are fixed.

β	HPM result [31]	HPM result [31]	Exact result [31]	Exact result [31]	Present result	Present result
	$-f''(0)$	$-g''(0)$	$-f''(0)$	$-g''(0)$	$-f''(0)$	$-g''(0)$
0.0	1.0	0.0	1.0	0.0	1.0	0.0
0.1	1.02025	0.06684	1.020259	0.066847	1.02026	0.06685
0.2	1.03949	0.14873	1.039495	0.148736	1.03949	0.14874
0.3	1.05795	0.24335	1.05794	0.243359	1.05795	0.24336
0.4	1.07578	0.34920	1.075788	0.349208	1.07578	0.34921
0.5	1.09309	0.46520	1.093095	0.465204	1.09309	0.46521
0.6	1.10994	0.59052	1.109946	0.590528	1.10994	0.59053
0.7	1.12639	0.72453	1.126397	0.724531	1.12639	0.72453
0.8	1.14248	0.86668	1.142488	0.866682	1.14249	0.86668
0.9	1.15825	1.01653	1.158253	1.016538	1.15826	1.016538
1.0	1.17372	1.17372	1.173720	1.173720	1.17372	1.17372

doi:10.1371/journal.pone.0105107.t002

Table 3. Comparision of results for the local Nusselt number $-\theta'(0)$ in the absence of non-Newtonian parameters and nanoparicles when $\beta=0$ with the work of Khan and Pop [15] and Nadeem and Hussain [32]

Pr	Present result	Khan and Pop [15]	Nadeem and Hussain [32]
0.07	0.066	0.066	0.066
0.20	0.169	0.169	0.169
0.70	0.454	0.454	0.454
2.0	0.911	0.911	0.911

doi:10.1371/journal.pone.0105107.t003

$$\beta_1=\lambda_1 a,\ \beta_2=\lambda_2 a,\ \beta=\frac{b}{a},\lambda=\frac{Q_0}{\rho a C_p},\ \Pr=\frac{\nu}{\alpha},$$
$$N_b=\frac{\tau D_B(C_w-C_\infty)}{\nu},N_t=\frac{\tau D_T(T_w-T_\infty)}{T_\infty \nu},Le=\frac{\alpha}{D_B}. \quad (15)$$

The physical quantities of interest are the local Nusselt number Nu_x and the local Sherwood number Sh_x, which are defined as

$$Nu_x=-\frac{x}{(T-T_\infty)}\left(\frac{\partial T}{\partial z}\right)\Big|_{z=0}, \quad (16)$$

$$Sh_x=-\frac{x}{(C_w-C_\infty)}\left(\frac{\partial C}{\partial z}\right)\Big|_{z=0}. \quad (17)$$

In terms of dimensionless form one has

$$Re^{-\frac{1}{2}}Nu_x=-\theta'(0),\ Re^{-\frac{1}{2}}Sh_x=-\phi'(0), \quad (18)$$

where $Re=ux/\nu$ is the local Reynolds number.

Convergence of the Homotopy Solutions

The problems containing non-linear coupled ordinary differential equations (19)–(12) subjected to boundary conditions (13)–(14) have been computed analytically by the homotopy analysis method (HAM). In the HAM role of the auxiliary parameters $\hbar_f$, $\hbar_g$, $\hbar_\theta$, and $\hbar_\varphi$ is of key importance because they control the convergence of the series solution. The most suitable value of these auxiliary parameters is calculated by considering minimum square error which is given by

$$F_{f,m}=\frac{1}{N+1}\sum_{j=0}^{N}\left[N_f\sum_{i=0}^{m}F_J(i\Delta\eta)\right]^2. \quad (19)$$

Table 1 ensure the convergence of the series solution which shows that the convergent solution for the velocity is obtained at 20th-order of approximation whereas such a convergence for temperature and concentration is achieved at 26th-order of approximation.

Numerical Results and Discussion

The aim of this section is to analyze the influence of the various physical parameters on the velocity, temperature and nanoparticle fields respectively. Figs. 1–14 are plotted to see the variation of the Deborah numbers β_1 and β_2, Prandtl number Pr, heat source ($\lambda>0$) or sink ($\lambda<0$) parameter, Brownian motion parameter N_b and thermophoresis parameter N_t on the fluid temperature and concentration fields.

Fig. 1 shows the influence of the Deborah number β_1 on the temperature field. By increasing Deborah number β_1 both the fluid temperature and thermal boundary layer thickness increases. This is due to fact that the Deborah number β_1 involves relaxation time λ_1. An increase in the relaxation time leads to increase in the temperature and boundary layer thickness. Fig. 2 illustrates the effects of the Deborah number β_2 on the temperature field. From this figure, it is noted that the behavior of the Deborah number β_2 is opposite to that of β_1. This is due to fact that the retardation time provides resistance which causes a reduction in the temperature and thermal boundary layer thickness. Fig. 3 presents the effects of the stretching parameter β on the fluid temperature $\theta(\eta)$. We observed that the temperature and thermal boundary layer thickness reduce with the increasing β. Fig. 4 illustrates the influence of the Prandtl number Pr on the temperature field. We

Table 4. Comparision of results for the local Nusselt number $-\theta'(0)$ and local Sherwood number $-\phi'(0)$ in the presence of nanoparticle of when $\beta=0, \beta_1=\beta_2=0.3, \lambda=0$, Pr $=6$ and $Le=1$ are fixed with the work of Nadeem et al. [33].

N_t	N_b	Present result	Present result	Nadeem et al. [33]	Nadeem et al. [33]
		$-\theta'(0)$	$\varphi'(0)$	$-\theta'(0)$	$\varphi'(0)$
0.3	0.3	0.33984	1.83994	0.33988	1.83935
0.5	0.3	0.24088	1.95813	0.24099	1.95862
0.3	0.5	0.14814	1.87029	0.14820	1.87035
0.5	0.5	0.10478	1.94565	0.10486	1.94572

doi:10.1371/journal.pone.0105107.t004

Table 5. Variations of the Local Nusselt number and local Sherwood number with β, Pr, λ, N_b, N_t and Le when $\beta_1 = \beta_2 = 0.2$ are fixed.

β	Pr	λ	N_b	N_t	Le	$-\theta'(0)$	$\varphi'(0)$
0.0	1.2	0.2	0.1	0.1	1.0	0.351853	0.474210
0.3						0.509837	0.482838
0.4						0.549438	0.488939
0.5	1.0					0.513728	0.430930
	1.1					0.551238	0.463216
	1.3					0.617393	0.527723
		0.0				0.757208	0.356670
		0.1				0.676907	0.422143
		0.4				0.335390	0.690221
			0.2			0.540514	0.683362
			0.3			0.497586	0.745281
			0.4			0.456841	0.775726
				0.2		0.575795	0.199343
				0.4		0.505394	−0.277762
				0.5		0.480757	−0.464410
					0.8	0.591165	0.352548
					0.9	0.588200	0.426414
					1.1	0.583427	0.560578

doi:10.1371/journal.pone.0105107.t005

observed that the temperature and thermal boundary layer thickness are reduced for large Prandtl number. Since thermal diffusivity is an agent which plays a key role for lower or higher temperature. Hence resulting larger value of the Prandtl number corresponds to diminishing of the thermal diffusivity resulting in a temperature decrease. Figs. 5 and 6 are plotted to analyze the effects of the heat source parameter (when $\lambda>0$) and heat sink parameter (when $\lambda<0$), respectively. It is observed that temperature of the fluid increases with the increase in the heat source parameter and an opposite behavior is observed for heat sink parameter. The influence of the Brownian motion parameter N_b and thermophoresis parameter N_t on the temperature is depicted through Figs. 7 and 8, respectively. It is observed that the temperature and thermal boundary layer thickness increases as the Brownian motion parameter N_b increases. Physically, this is due to the fact that with an increase of the Brownian motion parameter N_b the random motion of particle increases which results in an enhancement in the temperature profile. The temperature and thermal boundary layer thickness are detected to increase with an increase in thermophoresis parameter N_t (Fig. 8). In fact with the increase of the thermophoresis parameter N_t the difference between the wall temperature and reference temperature increases which causes increase in temperature profile.

In Figs. 9 and 10, we plotted the concentration profile for various values of the Deborah numbers β_1 and β_2, respectively. As the Deborah numbers β_1 increases, the concentration profile as well as concentration boundary layer thickness increase. However, the effects of β_2 on the concentration profile are quite opposite to that of β_1. Fig. 11 shows the influence of the heat generation parameter λ on the concentration profile. A decrease in the concentration profile and concentration boundary layer thickness near the plate is noted while the reverse effect is reported far away from the plate with the increasing value of the heat generation parameter λ. Fig. 12 illustrates the influence of the Lewis number Le on the concentration profile $\phi(\eta)$. It is noted that the concentration profile increases by increasing the Lewis number Le as Lewis number is inversely proportional to the diffusion coefficient. Thus an increase in Lewis number yields a decrease in diffusion which finally results in a decrease of mass fraction function $\vartheta(\eta)$. The variations with η of the concentration profile for different values of the Brownian motion parameter N_b and thermophoresis parameter N_t are presented in Figs. 13 and 14, respectively. In Fig. 13, it is observed that concentration profile increases with the increasing of the Brownian motion parameter N_b. This is due to the dependency of the concentration on the temperature field and we expect that a lower Brownian motion parameter allow a deeper penetration of the concentration. On the other hand, a qualitatively opposite trend in the concentration profile is observed as the thermophoresis parameter N_t increases. Further, it is noticed that the thermophoresis parameter N_t affects the concentration profile more than Brownian motion parameter N_b does.

Numerical values for the velocity gradients $-f''(0)$ and $-g''(0)$ are compared with the existing literature in the absence of both nanoparticles and non-Newtonian effects and shown in table 2, where they are found to be in excellent agreement, cementing the validity of the present results. Table 3 gives comparison of local Nusselt number $-\theta'(0)$ with the results obtained by Khan and Pop [15] and Nadeem and Hussain [32] Table 4 provides comparison of local Nusselt number $-\theta'(0)$ and local Sherwood number $-\vartheta'(0)$ for different values of the Brownian motion parameter N_b and the thermophoresis parameter N_t with existing results obtained by Nadeem *etal*.[33]. Table 5 is prepared for the variation of the local Nusselt number (heat transfer rate) and the local Sherwood number (concentration rate) for different values of the involved parameters. It is reported that the local Nusselt number $-\theta'(0)$ increases when β and $\mathbf{Pr}$ increase whereas it decreases as λ, N_b, N_t and Le increase. It is evident from table 5 that the local Sherwood number $-\phi'(0)$ increases with the increase of the parameters β, $\mathbf{Pr}$, λ, N_b and Le, however, it decreases with the increase of N_t.

Concluding Remarks

This study has analyzed the effects of the heat generation/absorption on three-dimensional flow of an Oldroyed-B nanofluid over a bidirectional stretching sheet. From the present investigation, the main observations were as follows:

- Qualitatively, effects of the Deborah numbers β_1 and β_2 on the temperature and concentration profiles were similar.
- The temperature profile as well as thermal boundary layer thickness were increased by increasing both the Brownian motion parameter N_b and thermophoresis parameter N_t.
- The temperature of the fluid and thermal boundary layer thickness is enhanced when there is a increase in the heat generation parameter λ.
- The concentration profile was decreased with the increase of the Brownian motion parameter N_b and a quite opposite behavior was noted with increasing thermophoresis parameter N_t.
- It was noted that the thermophoresis parameter N_t affected the concentration profile more than the Brownian motion parameter N_b did.
- An increase in the heat generation parameter (when $\lambda>0$) corresponds to reduction in the values of the local Nusselt number $-\theta'(0)$ while the opposite behavior is observed for the local Sherwood number $-\phi'(0)$.
- The magnitude of the local the local Nusselt number $-\theta'(0)$ decreases with the increase of the Brownian motion parameter N_b.
- The magnitude of the local the local Sherwood number $-\phi'(0)$ increase with the increase of the Brownian motion parameter N_b.

Acknowledgments

We are grateful to the reviewers for their constructive suggestions.

Author Contributions

Conceived and designed the experiments: MK WAK RM. Performed the experiments: MK WAK RM. Analyzed the data: MK WAK RM. Contributed reagents/materials/analysis tools: MK WAK RM. Wrote the paper: MK WAK RM.

References

1. Choi SUS (1995) Enhancing thermal conductivity of fluids with nanoparticles. ASME Int Mech Eng 66: 99–105.
2. Choi SUS, Zhang ZG, Yu W, Lockwood FE, Grulke EA (2001) Anomalously thermal conductivity enhancement in nanotube suspensions. Appl Phys Lett 79: 2252–2254.

3. Sakiadis BC (1961) Boundary layer behavior on continuous solid flat surfaces. J AIChE 7: 26–28.
4. Crane L (1970) Flow past a stretching plate. Z Angew Math Phys 21: 645–647.
5. Wang CY (1989) Free convection on a vertical stretching surface. Z Angew Math Mech 69: 418–420.
6. Elbashbeshy EMA (2001) Heat transfer over an exponentially stretching continuous surface with suction. Arch Mech 53: 643–651.
7. Rana GC, Kango SK (2011) Effect of rotation on thermal instability of compressible Walters' (model) elastico-viscous fluid in porous medium. JARAM, 3 (4): 44–57.
8. Ishak A, Nazar R, Pop I (2008) Heat transfer over a stretching surface with variable heat flux in micropolar fluids. Phys. Lett A 372: 559–561.
9. Chamkha AJ, Aly AM (2011) MHD free convection flow of a nanofluid past a vertical plate in the presence of heat generation or absorption effects. Chem Eng Commun 198: 425–441.
10. Rana GC (2013) Thermosolutal convection in Walters' (Model B') elastico-viscous rotating fluid permeated with suspended particles and variable gravity field in porous medium in hydromagnetics. J Appl Fluid Mech 6: 87–94.
11. Matin MH, Heirani MR, Nobari, Jahangiri P (2012) Entropy analysis in mixed convection MHD flow of nanofluid over a non-linear stretching sheet. J Therm Sci Technol 7:104–119.
12. Chand R, Rana GC (2012) Oscillating convection of nanofluid in porous medium. Transport in Porous Media 95: 269–284.
13. Aziz A, Khan WA (2012) Natural convective boundary layer flow of a nanofluid past a convectively heated vertical plate. Int J Therm Sci 52: 83–90.
14. Kuznetsov AV, Nield DA (2010) Natural convective boundary- layer flow of a nanofluid past a vertical plate. Int J Therm Sci 49: 243–247.
15. Khan WA, Pop I (2010) Boundary-layer flow of a nanofluid past a stretching sheet. Int J Heat Mass Transf 53: 2477–2483.
16. Khan WA, Pop I (2011) Free convection boundary layer flow past a horizontal flat plate embedded in a porous medium filled with a nanofluid. J Heat Transf 133: 9.
17. Hamad MAA, Pop I, Ismail AI (2011) Magnetic field effects on free convection flow of a nanofluid past a semi-infinite vertical flat plate. Nonlinear Anal: Real World Appl 12: 1338–1346.
18. Hady FM, Ibrahim FS, Abdel-Gaied SM, Eid MR (2012) Radiation effect on viscous flow of a nanofluid and heat transfer over a nonlinearly stretching sheet. Nanoscale Res Lett 7: 229.
19. Makinde OD, Aziz A (2011) Boundary layer flow of a nanofluid past a stretching sheet with a convective boundary condition. Int J Therm Sci 50: 1326–1332.
20. Cheng C-Y (2012) Free convection boundary layer flow over a horizontal cylinder of elliptic cross section in porous media saturated by a nanofluid. Int Commun Heat Mass Transf 39: 931–936.
21. Narayana M, Sibanda P (2012) Laminar flow of a nanoliquid film over an unsteady stretching sheet. Int J Heat Mass Transf 55: 7552–7560.
22. Kameswaran PK, Narayana N, Sibanda P, Murthy PVSN (2012) Hydromagnetic nanofluid flow due to a stretching or shrinking sheet with viscous dissipation and chemical reaction effects. Int J Heat Mass Transf 55: 7587–7595.
23. Bachok N, Ishak A, Pop I (2012) Unsteady boundary-layer flow and heat transfer of a nanofluid over a permeable stretching/shrinking sheet. Int J Heat Mass Transf 55: 2102–2109.
24. Hamad MAA, Ferdows M (2012) Similarity solutions to viscous flow and heat transfer of nanofluid over nonlinearly stretching sheet. Appl Math Mech 33 (2012) 923–930.
25. Alsaedi A, Awais M, Hayat T (2012) Effects of heat generation/absorption on a stagnation point flow of nanofluid over a surface with convective boundary conditions. Commun Nonlinear Sci Numer Simulat 17: 4210–4223.
26. Chand R, Rana GC (2012) Thermal instability of Rivlin—Ericksen elastico-viscous nanofluid saturated by a porous medium. J Fluids Eng 134 (12): 121203.
27. Chand R, Rana GC (2012) On the onset of thermal convection in rotating nanofluid layer saturating a Darcy–Brinkman porous medium. Int J Heat Mass Transf 55: 5417–5424.
28. Nandy SK, Mahaparta TR (2013) Effects of slip and heat generation/absorption on MHD stagnation point flow of nanofluid past a stretching/shrinking surface with convective boundary conditions. Int Heat Mass Transf 64: 1091–1100.
29. Rana GC, Thakur RC, Kango SK (2014) On the onset of thermosolutal instability in a layer of an Elastico-Viscous nanofluid in porous medium. FME Transactions 42: 1–9.
30. Ariel PD (2007) The three-dimensional flow past a stretching sheet and the homotopy perturbation. Comput Math Appl 54: 920–925.
31. Shehzad SA, Alsaedi A, Hayat T, Alhuthali MS (2013) Three-dimensional flow of an Oldroyd-B fluid with variable thermal conductivity and heat generation/absorption. PLOS One, 8 (11): e78240.
32. Nadeem S, Hussain ST (2013) Flow and heat transfer analysis of Williamson nanofluid. Appl Nanosci doi 10.1007/s13204-013-0282-1.
33. Nadeem S, Haq RU, Akbar NS, Lee C, Khan ZH (2013) Numerical study of boundary layer flow and heat transfer of Oldroyd-B nanofluid towards a stretching sheet. PLOS One, 8(8): e69811.